GPS Solut (2009) 13:173–182
DOI 10.1007/s10291-008-0110-3

ORIGINAL ARTICLE

Kalman-filter-based GPS clock estimation for near real-time positioning

André Hauschild · Oliver Montenbruck

Received: 28 July 2008 / Accepted: 28 October 2008 / Published online: 16 November 2008

Abstract In this article, an algorithm for clock offset estimation of the GPS satellites is presented. The algorithm is based on a Kalman-filter and processes undifferenced code and carrier-phase measurements of a global tracking network. The clock offset and drift of the satellite clocks are estimated along with tracking station clock offsets, tropospheric zenith path delay and carrier-phase ambiguities. The article provides a brief overview of already existing near-real-time and real-time clock products. The filter algorithm and data processing scheme is presented. Finally, the accuracy of the orbit and clock product is assessed with a precise orbit determination of the MetOp satellite and compared to results gained with other real-time products.

Keywords Clock estimation · Precise orbit determination · Real-time · Kalman filter

Introduction

A growing number of near real-time precise point positioning (PPP) applications raise the need for precise GPS orbit and clock products with short latency. One of these applications is the precise orbit determination (POD) of remote-sensing satellites, which is to be performed shortly after a ground station pass. The observations of the satellite's GPS receiver are available immediately after the download to the ground station. For processing these data, the user requires precise orbit and clock data for the complete GPS constellation. The rubidium and cesium atomic standards of the GPS satellites are subject to clock noise and frequency variations, which can originate from a variety of effects and are hard to forecast. Predictions of clock offset and drift, which are provided for example in the predicted part of the ultra-rapid orbits provided by IGS or the broadcast ephemerides, will deviate quickly from the true values by several decimeters or even meters. Thus, these orbit/clock-products become unusable for PPP applications, where a carrier-phase based positioning accuracy down to centimeter level is desired. The solution to this problem is the use of clock offsets, which have been estimated from GPS measurements originating from a network of sensor stations. Currently, only a limited set of providers for precise (near-) real-time orbit/clock-products is available. Among them are three of the IGS Analysis Centers: JPL (Bar-Sever et al. 2003), NRCan and ESA (Pérez et al. 2006). The JPL products are transmitted to the user with a latency of about 5 s and can be accessed in various ways, for example, internet data streams and satellite broadcast. The real-time orbit and clock product generation at ESA is currently under development and not publicly available. For our article, however, near real-time orbit and clock products dedicated for the support of the MetOp-Mission have been used. A batch algorithm has been used to generate these products by processing a 2-day data arc for the satellite orbits. The corresponding clocks are computed from shorter data arcs of 23 min including an overlap of 8 min to the previous batch (Zandbergen et al. 2006). The real-time orbits and clocks from NRCan are based on data from a global real-time station network. The products are not publicly available.

The Astronomical Institute of University Berne (AIUB) has also computed near-real-time clock and orbit products for the test period used in this article. AIBU generates

A. Hauschild (✉) · O. Montenbruck
German Space Operations Center (GSOC),
Deutsches Zentrum für Luft-und Raumfahrt (DLR),
82234 Wessling, Germany
e-mail: andre.hauschild@dlr.de

orbit- and clock-data by post-processing of short 100-min-batches of GPS observations (Bock et al. 2008).

A real-time system for clock estimation is currently under development at the German Space Operations Center of DLR. The generated orbit/clock-products will be used to support orbit determination of low-earth-orbit satellites (LEO satellites) for up-coming space missions, which require near real-time orbit determination accuracies down to 8–10 cm. The software is based on a Kalman-filter, which processes undifferenced code and carrier phase observations from a worldwide network of GPS stations. The filter uses the orbit information from the predicted part of the latest ultra-rapid IGS products and estimates clock offsets and drifts for the complete GPS constellation. In this article, the complete filter algorithm including the pre-processing of the raw measurements is introduced. The orbit and clock products computed with the filter algorithm are used for a POD with real GPS measurements from the GNSS Receiver for Atmospheric Sounding (GRAS) onboard the MetOp-A satellite. The same analysis has also been performed with the IGS ultra-rapid, JPL, ESA and AIUB products and the results are compared and discussed.

Filter algorithm

The clock-estimation algorithm is based on a Kalman-filter, which can be used as a conventional Kalman-filter as well as a forward-/backward-filter with smoother. The filter processes ionosphere-free linear data combinations of code and carrier phase measurements on the L1- and L2-frequency. The filter state includes the satellite clock error and the clock drift for the complete constellation of 32 satellites.

The state vector additionally comprises the receiver clock offset, a differential tropospheric zenith delay as well as the float carrier phase ambiguities of all satellites in view of each station. The station positions are extracted from recent IGS Sinex-files (IGS 2008) and held fixed in the filter. The current GPS constellation has 32 active satellites and typical tracking network size for the filter is about 20 stations. Assuming that each station tracks on average 10 GPS satellites leads to a total number of about 300 elements in the state vector.

Some of the state vector elements require further explanation: the estimated receiver clock offsets for the tracking stations do not represent the offset of the real receiver clocks, since the observation data has been pre-processed before being used in the filter. The pseudo range observations are used together with the a priori orbits and known station position to compute a coarse estimation of the receiver's clock error. All observations and the measurement epoch are then corrected by the estimated clock offset. This pre-processing reduces large clock jumps in the order of milliseconds to less then a microsecond and is beneficial for two reasons: first, the process noise for the receiver clocks can be reduced by several orders of magnitude, as ground station clock jumps do not have to be compensated for. It has been found that this procedure improved the filter stability during measurement updates. Second, elimination during pre-processing eases the filter implementation in later filter steps, as no further measures are necessary for a consistent handling of the ground station clocks. In addition, individual process noise settings for each ground station are avoided, which would need to be maintained in case of changes in the station setup. The differential tropospheric zenith delay shall also be explained in further detail here. The model of the ionosphere-free code and carrier phase observables already includes corrections for the tropospheric delay using a model of the standard atmosphere, which will be introduced later in this section. The true tropospheric delay will differ from the values provided by the empirical model, since the actual local weather conditions deviate from the model parameters. To compensate these deviations, a differential zenith path delay is estimated for each station, which is then mapped into a differential tropospheric slant delay, using an elevation dependent mapping function. The carrier phase ambiguities in the filter state are estimated as float values and are not fixed.

In order to be able to perform the Kalman-filter time update, the state vector must be predicted towards the next update epoch using a system model. For this algorithm, the GPS satellite clocks are predicted linearly in time. The clock drift and all other state parameters are assumed to be constant. Of course, the satellite clock drift is not strictly constant but it undergoes slow variations. These variations are due to the characteristics of the individual satellite clocks and are driven by hardly predictable effects like thermal variations onboard the GPS satellites. Furthermore, the ground station clock offset and the differential tropospheric delay are subject to variations. In order to compensate the deviations of the system model from the truth, process noise is introduced on these elements of the state vector. Without process noise, the covariance of the state vector would decrease over time and as a result, the weight of the measurements during the filter update decreases, which leads to divergence of the filter.

Figure 1 depicts a flowchart of the complete filter algorithm. At the beginning, the forward filter is initialized. The coarse values from the IGS ultra-rapid product are used as a priori values for the satellite clock offset and drift. All other elements of the state vector are set to zero. Additionally the process noise for the filter state and the measurement noise are set during this step.

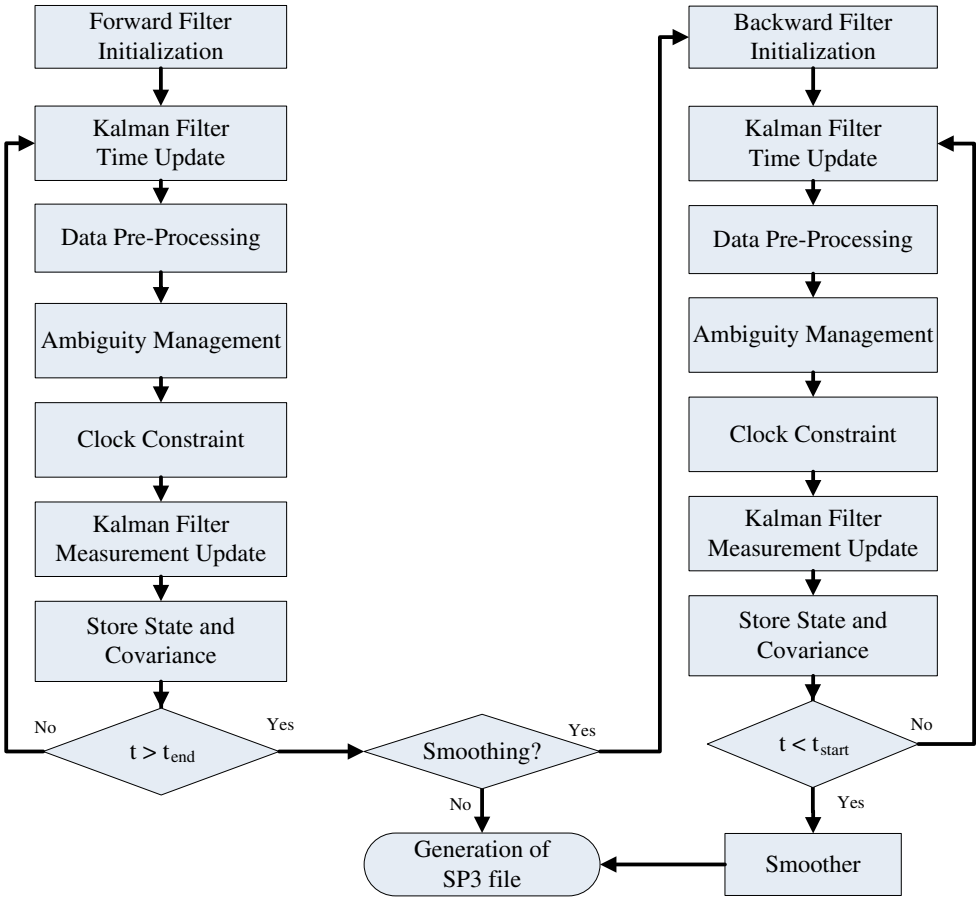

Fig. 1 Flowchart of the clock-estimation algorithm

The selection of the process noise and measurement noise determines whether the filter adds more weight to the propagated state based on the system model or to the actual measurements. That is, if the process noise is low compared to the measurement noise, the filter will rely more on the system model and will only gradually correct the filter state during the measurement update. Meaningful settings for the noise of the observables can easily be found from an assessment of the measurement precision. In our case, the carrier phase observables have been assigned a measurement noise of 2 cm. This value also takes the effect of possible multipath errors at a cutoff angle of 10° into account. The code observables have been weighted with a measurement noise of 2 m.

The process noise of the state vector elements is in general more difficult to determine. For simplicity, it is assumed to result from an integrated white noise process, which means that the process noise increases linear in time. It is denoted q_i for the filter state element i and is characterized with the standard deviation σ and a time constant τ. The process noise matrix has diagonal structure and the elements of the main diagonal are found from

$$q_i = \sigma_i^2 \frac{\Delta t}{\tau_i}. \quad (1)$$

The time difference Δt denotes the time between the consecutive epochs.

For the process noise settings of the satellite clock states, no distinction is made between the individual clock types. Instead, the process noise settings are the same for all GPS satellites. The clock offsets have a process noise with a standard deviation of 3 cm and a time-constant of 600 s. The clock drift process noise has a standard deviation of 0.0005 m/s ($\approx 10^{-12}$ s/s) over 900 s. Though these simplified assumptions do not strictly reflect the selected two-state clock-model, they are favored for a real-time capable process compared to more elaborated models. Using clock models with characteristic process noise settings depending on the satellite block type (Senior et al. 2008) or even on the individual satellite clocks (Hutsell 1996) adds more complexity, since changes of the used onboard frequency standard or untypical clock behavior must be detected to adjust the process noise settings. Otherwise, the benefits of the model would not be fully exploited. Adapting the settings in real-time from recent

data significantly increases the computational load and has therefore not been attempted. However, a rigor assessment of the benefits different clock models deems helpful to identify possible enhancements.

The differential zenith path delay of the ground stations are assumed to vary only marginally over time. Consequently, only a small amount of process noise with a standard deviation of 2 mm over 1 h is assigned. On the contrary, the ground station clock offset will exhibit noise-like behavior with deviations in the order of tens of meters due to the "clock-jump" elimination procedure mentioned previously. Therefore, the comparably large process noise has been chosen to compensate for these deviations. The ambiguities of the carrier phase measurements are assumed to be constant parameters and therefore no process noise is introduced. Upon filter initialization, the initial covariance matrix is set up as a diagonal matrix with the square of the initial standard deviation on the main diagonal. Table 1 provides an overview of the filter settings.

In the next step, the filter state is propagated towards the first epoch where measurements are available. During pre-processing in the following step, the ground station clock jumps are eliminated from the data as previously explained. Additionally, the observables are screened for missing data and satellites, which have dropped below an elevation cutoff angle of 10°. The core part of the data screening is an integrity monitoring which is performed on the pseudo range and the carrier phase measurements in order to detect and remove outliers. During this monitoring, the orbits and clocks of the predicted IGU product are used together with the known station position to compute the residuals of the ionosphere-free observations for each satellite. Since the position is known, only the station clock offset, which is common for all measurements, must be computed and removed from the residuals. If the RMS of the pseudo ranges exceeds a predefined threshold, the residuals are recursively recomputed with a single satellite excluded at a time. The combination, which yields the lowest residual, identifies the satellite with the outlier in the pseudo range measurement. This satellite is excluded from the filter at this epoch. If the residual-threshold is still exceeded, the procedure of recursively excluding satellite is repeated until the threshold is met or the number of valid satellites drops to two. In the latter case, all remaining satellites are rejected as well, since the monitoring procedure cannot further be performed. A similar approach has been chosen for the monitoring and screening of the carrier phase measurements, but instead time differences of the carrier phases between the current and the previous epoch are used, in order to avoid the complication of estimating ambiguities at this step. With this monitoring procedure, measurement outliers and cycle slips can be detected and the associated satellites are excluded from the measurement update.

Table 1 Settings for initial covariance matrix, process noise and measurement noise

Parameter	A priori SD σ_0	SD σ	Time scale τ (s)
Filter State			
GPS clock offset	2 m	0.03 m	600
GPS clock drift	0.005 m/s	0.0005 m/s	900
Rcv clock offset	100 m	500 m	100
Zenith delay	0.5 m	0.002 m	3,600
Ambiguity	5 m	–	–
Measurement noise			
Pseudo range	–	2 m	–
Carrier phase	–	0.02 m	–
Clock constraint	–	0.1 m	–

Afterwards, the ambiguities in the state vector are examined. If satellites have dropped below the elevation limit of the filter or are no longer tracked, their ambiguities are deleted and the space in the filter state is freed. If satellites are newly acquired, their ambiguities are initialized using code-carrier differences to provide their initial values. In addition, ambiguities of satellites, which have been rejected during the data screening, are removed from the filter and initialized again as soon as valid measurements for the satellite are available.

Prior to the measurement update the filter applies a clock constraint, since the mean of all GPS satellite clocks is unobservable in the system. The clock constraint is applied as a "pseudo"-measurement update, which treats the mean of all clock offsets in the IGU clock product as observation of the mean clock offset in the filter state. Therefore, the filter clock estimates are tied to the predicted mean IGU clock, which is serves as a virtual reference clock.

Special care has been taken in modeling the pseudo range and carrier phase observations in the measurement update. Table 2 summarizes the used models and conventions. After the measurement update of the filter, the state vector and the associated covariance matrix are stored for potential usage in the smoother. The procedure is iterated until all epochs have been processed. If smoothing of the results is not desired, they are stored in an SP3-file, which consists of the ultra-rapid orbit interpolated to 30 s intervals. The original clock parameters from the ultra-rapid file are replaced by the filter results.

If the smoother shall be used, the filter is again initialized to process the complete data arc backwards in time starting at the end. The processing scheme is identical to the forward filter. After the backward run is finished, the smoother computes the mean of the forward and backward results of the filter state weighted according to their

Table 2 Modeling of pseudo range and carrier phase observations

Model		Reference
Station position	Earth tides	McCarthy and Petit (2004)
	Pole tides	McCarthy and Petit (2004)
	Ocean loading	McCarthy and Petit (2004)
Tropospheric delay	UNB model	Collins et al. (1996)
C1P2 Ionosphere free combinations	P1C1 differential Code biases	Schaer and Steigenberger (2006)
Phase center offsets/variations	IGS 05 Conventions	Schmid et al. (2007)
Phase wind up	Phase wind up Correction	Wu et al. (1993)

covariance. The filter requires some time after initialization during which the filter state converges and the computed covariance decreases. Consequently, at the beginning of the data interval, the bad estimates of the forward filter are weighted less than the better estimates of the backward filter and vice versa. Forward/backward-smoothing thus reduces the sensitivity of the filter towards convergence errors especially for short data arcs, where the convergence time of the filter is a significant fraction of the complete data arc.

correction and do not affect the position. Therefore, these common errors must be eliminated from the SISRE at each epoch. The computation of the SISRE for a single satellite i is based on the cross-track and along-track orbit errors denoted as e_C and e_A, respectively, and the combined radial orbit and clock error $e_{\mathrm{RE/CE}}$. The mean of the latter error is denoted $\overline{e}_{\mathrm{RE/CE}}$. It is the quantity to be eliminated at each epoch.

Using these expressions, the equation for the modified signal in space range error is found:

$$\mathrm{SISRE}^{(i)} = \sqrt{\mathrm{RMS}^2\left(\left(e^{(i)}_{\mathrm{RE/CE}} - \overline{e}_{\mathrm{RE/CE}}\right)\right) + \frac{1}{49}\left(\mathrm{RMS}^2\left(e^{(i)}_{C}\right) + \mathrm{RMS}^2\left(e^{(i)}_{A}\right)\right)}. \quad (2)$$

The capabilities of this clock filter algorithm are two-fold: it can be used to compute clock solutions for a given orbit product based on recorded global GPS observations for long and short data arcs. It can also be used to demonstrate the expected performance of a real-time clock estimation filter, by using it as a standard forward Kalman filter. The typical processing time of the algorithm with a 20 station network and clock solutions at 30 s epochs is about 1 h on a recent office PC for a forward-only solution. The data sources used for this analysis are accumulated daily Rinex-files downloaded from the IGS data archive.

Clock product assessment strategy

Having computed an orbit- and clock-product immediately poses the question how its performance in a position application can best be assessed. The Signal In Space Range Error (SISRE) has often been used to gain a coarse estimate of the expected positioning accuracy (Warren and Raquet 2003). The SISRE equation has been modified for the analysis of this article to avoid, that radial orbit errors or clock errors, which are common to all satellites, affect the computed SISRE. In a navigation solution, these common errors would be absorbed into the user clock

In this equation, the *RMS*()-terms denote the values of many individual errors over the time interval of interest. Since the combined error in the satellite clock and the radial orbit error have a larger impact on the user ranging error than the orbit error in cross-track and along-directions, they are scaled by a factor of 1/49. It should also be noted that for the clock error, the corresponding GPS antenna offsets, which have been used in the product generation, must be taken into account.

Complementary to the SISRE computation, the orbit and clock product have also been used in a LEO-satellite orbit determination. An iterated least-squares estimator implemented in the "GPS High Precision Orbit Determination Tools" (GHOST) has been utilized for this analysis. The batch algorithm provides estimates of the satellite's position and velocity, coefficients for the atmospheric drag and solar radiation pressure acting on the satellite, the receiver clock offset and the carrier phase ambiguities. Additionally, empirical accelerations are estimated which compensate un-modeled perturbation forces. The filter uses a reduced dynamical model for the satellite's trajectory. In the following, this batch algorithm will be referred to as Reduced-Dynamic Orbit Determination-tool (RDOD) (Montenbruck et al. 2005). It is important to note that the algorithm

estimates float values for carrier phase ambiguities. If sufficient data is available for a reliable estimation of the ambiguities, the carrier phase measurements have a dominating impact on the results compared to the pseudo range measurements. The resulting benefits will become visible during the discussion of the clock product comparison.

Results of clock product comparisons

The results obtained from the assessment of the clock and orbit product are presented and discussed in this section. First, the SISRE is computed according to the equations presented in the previous section. The reference solution for the SISRE computation is the final orbit- and clock-product with 30 s epochs obtained from the Center of Orbit Determination in Europe (CODE). In addition to this traditional measure, the RDOD-tool is used to perform a complete orbit determination of the MetOp-A satellite (Montenbruck et al. 2008). Again, the CODE orbits and clocks were used as reference for the comparison of five different orbit- and clock-products. Prior to discussing the analysis scheme, the origin of the different clock products shall be discussed in greater detail. The AIUB-product originates from a short-arc batch data processing with the Bernese software (Dach et al. 2007), which is also routinely used to produce the daily, high precision GPS orbit and clock products. The software has been setup to process 90-min batches of global observation data, which are obtained from the IGS high-rate network with a latency of about 1 h (Bock et al. 2008).

The JPL clocks are determined using a Kalman filter. This sequential filter is provided with real-time data streams of a global network and provides orbit and clock data at intervals of 60 s (Bar-Sever et al. 2003). In this analysis, the JPL clocks are the only product generated in real-time with a sequential filter. The ESOC orbit and clocks are dedicated products to support the POD as well as the scientific occultation experiments of the MetOp satellite. Data processing is done using a batch data processing scheme. ESOC processes data batches of 23 min with an 8 min overlap of consecutive batches. The clock solutions are based on already existing orbits and have a step size of 30 s (Zandbergen et al. 2006).

Finally, the IGS ultra-rapid (IGU) predicted orbits have also been used in this analysis. The IGU orbit cover an interval of 48 h, where the first 24 h are based on observations and the following 24 h are predicted orbits and clocks. The orbits are currently updated four times each day at 3, 9, 15 and 21 h UTC and have a latency of 3 h relative to the last observations. Since the accuracy of the predicted orbits and especially the clocks degrades with an increasing interval to the end of the observed data arc, the most recent product should be used as soon as it becomes available. Therefore, the IGU orbits have been concatenated at 3, 9, 15 and 21 h, respectively. Additionally, a cosine-weighted interpolation is used to fade-out the old orbit and clock and fade-in the new product. Thereby, discontinuities in the orbit product are reduced.

The DLR clocks are computed using the Kalman filter described in the previous sections. For test purposes, the filter has been used in forward only mode as required for a real-time application and, furthermore, with additional forward-backward smoothing of the filtered results. The clock parameters are computed based on the interpolated IGU-orbit data. Figure 2 depicts the station network that has been selected for the computation of the DLR clock products. The figure also depicts the visibility conditions assuming a 10° elevation mask. Light colors indicate that a

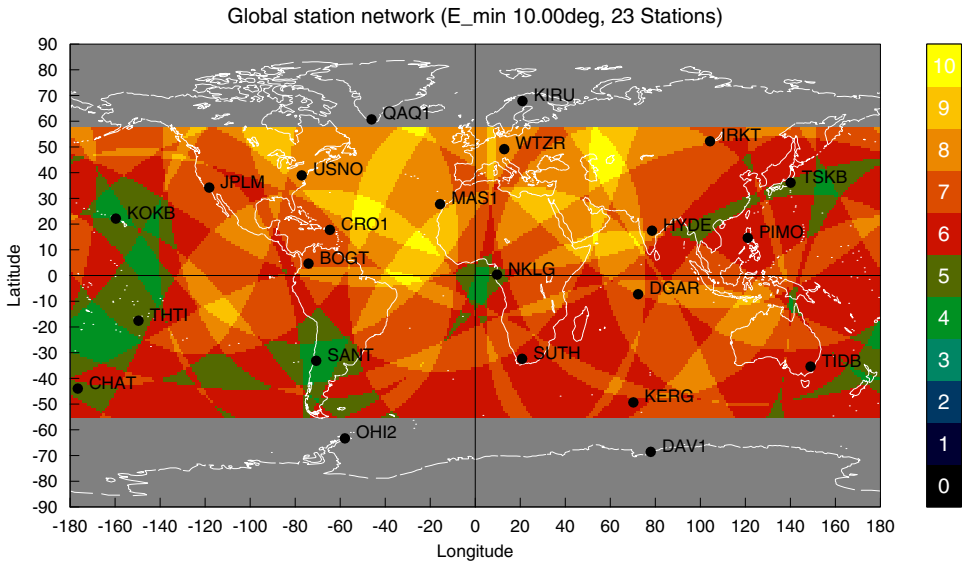

Fig. 2 Distribution and satellite visibility of the global station network selected for DLR clock solution

Table 3 SISRE and MetOp-A POD results for different GPS orbit and clock products, Epoch: 2006/12/26, 24 h-POD

Product	SISRE (mm)	RMS CP residual (mm)	3D position residual (mm)	Passes
CODE final	–	6.0	–	398
AIUB	135	7.5	26	426
DLR smoothed	47	13.0	34	385
DLR	65	14.0	45	385
ESOC	89	18.0	63	377
JPL	90	24.0	78	393
IGU	720	50.0	240	470

large number of stations can track a satellite; dark colors mean bad visibility conditions. The station distribution has been chosen to optimize the global visibility of the GPS satellites. With 23 stations in total, the network is smaller than the ones used for other orbit and clock products, but the size corresponds to the amount of stations currently available in real-time.

The output of the POD algorithm is a SP3-file containing the spacecraft positions and the receiver clock offsets. The MetOp-A-orbit solutions obtained for the various near real-time products are then compared to the orbit solution obtained with the CODE reference product. The RMS of the 3D-position residuals indicates the overall quality of the orbit determination. Additionally, a comparison of the residuals of the carrier phase observables for the clock product with the reference provides valuable information about the quality of the clock parameters.

The results for the long-arc data analysis are summarized in Table 3 which shows the SISRE, RMS carrier phase residuals, RMS 3D position residuals and the number of GPS satellite passes. The latter value originates also from the RDOD algorithm and is the amount of tracking arcs with continuous carrier phase observables.

At the beginning the discussion, the results for the SISRE are considered. As expected, the SISRE for the IGU orbit and clocks is largest with 72 cm. The AIUB clock products produce a notably improved SISRE with 13.5 cm. JPL and ESOC have virtually identical values of about 9.0 cm. The lowest SISRE is obtained for the DLR product with 6.5 cm, or 4.7 cm if smoothing is activated. Surprisingly, the comparison of the positioning accuracy and the SISRE indicates, that both performance measures disagree in certain cases. The positioning residuals show that the AIUB products supersede all other products. The second best positioning results are achieved with the DLR clocks. The ratio of 45 mm residuals for the sequential filter results to 34 mm to the smoothed results is approximately the same as the ratio of the respective SISRE-values. The ESOC and JPL products reach accuracies of 63 and 78 mm, respectively. As expected, the use of the IGS ultra-rapid orbit yields by far the worst results with 24 cm residuals. The residuals of the carrier phase observables have the same ranking as the position residuals. It is interesting to note that the AIUB product reaches almost the same level of carrier phase residuals as the reference product. This can be attributed to the fact that basically the same high precision algorithm is used in both cases, with the difference that the CODE final product was generated using a 24 h data arc compared to about 100 min for the near real-time product.

The first result from this analysis is that the SISRE obviously fails in certain cases to properly indicate the quality of an orbit/clock product for positioning applications. The AIUB product has the highest SISRE values, but it yields the best results when used for positioning. The reason for this phenomenon becomes obvious from a closer look at the satellite clocks as computed by AIUB. Figure 3 depicts the clock offsets for four GPS satellites from this product. The mean offset over all clocks in the constellation and the linear clock drift of each clock have been removed. It can be seen that all four clocks exhibit "clock jumps" in the order of a few decimeters at identical epochs. The length of the clock fragments is 90 min, which reflects the length of the processed data arcs. Similar clock discontinuities at the same epochs can also be seen for all other satellites in the constellation.

Obviously, the batch algorithm does not ensure consistency of the clock products with the previous batch. Instead, offsets in the order of decimeters, which change between consecutive runs of the algorithm and cannot be absorbed into the constellation mean clock offset, are induced into the clock parameters. However, the accuracy of the 24 h-orbit determination is not largely affected by these inconsistencies since the estimation relies to a large extent on the carrier phase measurements. The RDOD algorithm estimates carrier phase ambiguities for each observed satellite and uninterrupted tracking arc. The individual offset for each satellite clock is then absorbed into the estimated carrier phase ambiguity. With increasing tracking time, the covariance of the estimated ambiguities decreases and the precise carrier phase measurements gain larger impact on the POD solution. The pseudo ranges on the other hand are directly affected by the clock offsets in the AIUB product, but due to the higher measurement noise and lower weighting, the impact during the measurement update is lower. The clock jumps are compensated by the RDOD algorithm, since they appear as discontinuities of the carrier phase measurements. During data editing (see Montenbruck et al. 2005), these discontinuities are interpreted as carrier phase cycle slips and the ambiguity estimation is re-initialized again for the affected satellite. These events manifest themselves in an increased number of passes for the AIUB product. The last column in Table 3

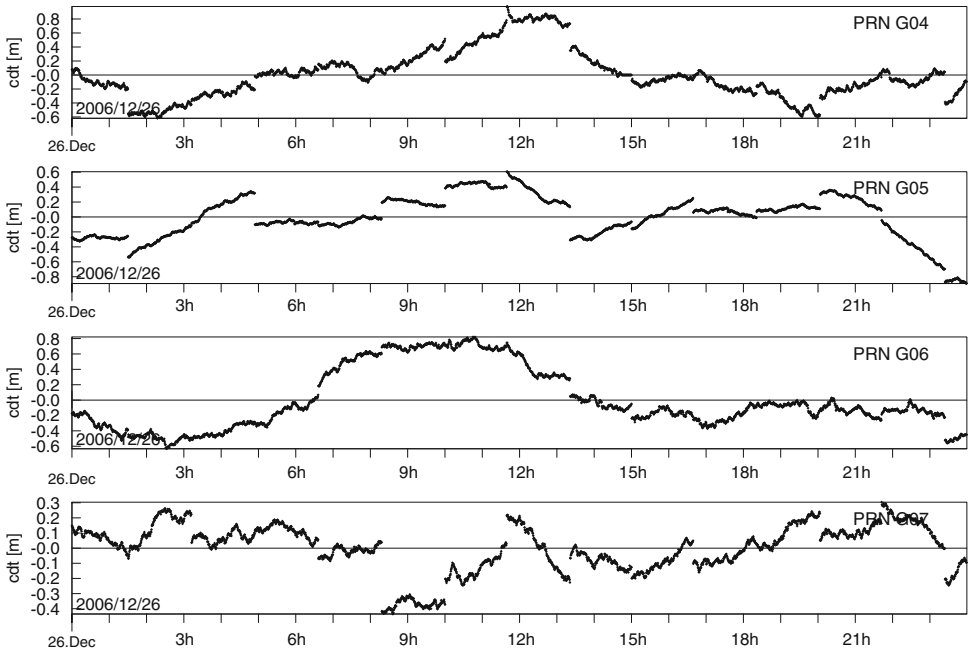

Fig. 3 Clock offsets for PRN 4, 5, 6 and 7 plotted from the AIUB clock product, mean constellation offset and linear drift have been removed

shows the number of satellite passes with continuous carrier phase observations. The AIUB product shows a significant increase in passes compared to the other products (with the IGU orbit being the exception due to its bad overall quality of clock prediction). The SISRE on the other hand is directly affected by the clock biases and jumps of the AIUB product, since it reflects the combined orbit and clock errors. As a result, the SISRE corresponds to the accuracy that would be gained if the clock discontinuities were not compensated for.

The DLR and JPL products originate from sequential processing algorithms and are not at risk of having problems with discontinuities, provided that the filter is not re-initialized. Consequently, the SISREs for these orbit and clocks reflect the real positioning accuracy. The comparable number of passes in Table 3 for these two products supports this conclusion.

Finally, the ESOC product, which is created with a batch least squares algorithm, has a SISRE comparable to the JPL clocks and a slightly poorer positioning accuracy. Obviously, the corrections for the individual satellite clocks in this product are consistent and not biased. It is interesting to note that this product reaches the lowest number of passes. This is due to the fact that the product provides orbits and clocks for only 28 satellites instead of 30 as all other products in this test. Still, the low number of passes indicates that the clocks do not exhibit a large amount of clock jumps. In contrary to AIUB, ESOC uses 23-min data arcs with overlapping 8 min for the generation of clock products. Consistency between the estimated clocks is assured by using the estimated ambiguities to initialize the ambiguities of the consecutive batch (Tim Springer, ESA/ESOC, private communication).

The previous analysis provides valuable insights into the advantages and disadvantages of the different clock products. A 24 h arc data analysis has been chosen to point out the problems caused by fragmentation of clock solutions. A more realistic scenario for near real-time orbit determination, however, is short-arc data processing. The measurements of the spacecraft's GPS receiver are available shortly after the transmission to the ground station. Data batches of approximately 90 min must be processed, assuming that the satellite dumps its data to the ground-station network once each orbit. Therefore, the same analysis has been repeated using short batches of observations between 90 and 100 min, resulting in 15 POD runs for each product. Table 4 summarizes the results. This time the SISRE and the number of passes are not displayed. The

Table 4 SISRE and POD residuals for the MetOp-A-satellite, Epoch: 2006/12/26, results are the mean and standard-deviation of 15 POD runs with 1.5 h data batches

Product	RMS CP Residual (mm)	3D position residual (mm)
CODE final	5.5 ± 0.5	21.9 ± 13.6
AIUB	6.8 ± 1.3	34.8 ± 14.3
DLR smoothed	9.0 ± 2.6	41.2 ± 16.0
DLR	11.0 ± 3.6	51.3 ± 34.0
ESOC	15.3 ± 1.9	88.4 ± 42.3
JPL	20.8 ± 3.0	113.9 ± 15.5
IGU	45.8 ± 8.3	350.0 ± 271.5

values for the carrier phase residuals and the position residuals are the mean and standard deviation of the 15 individual RDOD runs. The reference orbit for this analysis is again the MetOp-A orbit obtained for the 24 h analysis, since it is the most accurate solution.

In the second analysis, the accuracy of the orbit determination results is worse for all products. This decreased performance is expected since less information is available in the estimation process due to the reduced length of the data arc. The effect on the positioning accuracy can be demonstrated by inspection of the position residuals of the CODE final orbit for the short-arc analysis compared to the long arc analysis. The position shows mean residuals of approximately 2 cm. All other orbit and clock products show similar degradations in positioning accuracy for the short arc analysis. However, all products still achieve decimeter accuracy. As expected, the relative performance of the individual products is still the same as in Table 3.

Summary and conclusions

The Kalman filter for GPS satellite clock estimation developed at DLR/GSOC has been introduced in this article. Clock products generated with this filter are used along with other products for a POD of the MetOp-A-satellite for both long and short data arcs. For an initial assessment of the expected accuracy, the SISRE for the various orbit and clock products has been computed. The SISRE computation has been adapted to account for constellation-wide offsets in the radial directions, which do not affect the positioning solution. For carrier phase-based processing, however, the real accuracy of the product can significantly exceed the estimated accuracy indicated by the SISRE. It is therefore recommendable to further improve the SISRE computation to remove this flaw from this otherwise convenient and quick measure for orbit/clock product accuracy.

The comparison and discussion of the POD results of the various orbit and clock products showed that all products reach positioning accuracies at the decimeter level and below. The highest positional accuracy is gained with the AIUB product. This is an expected result, since the processing algorithm is closely related to the software package used for the generation of the final CODE orbits and clocks. However, the product contains clock biases and discontinuities. With the removal of these discontinuities, the performance of the product can be expected to increase even further. The second best results are gained using the DLR product. The clock results improve significantly if the algorithm uses forward/backward filtering. This improvement indicates that there exists a significant effect due to filter convergence in the clock solution, which could be further mitigated by starting the filter a few hours ahead of the first measurement epoch to be processed. The clock products computed by ESOC originate from a batch algorithm, but clock discontinuities are avoided here, since consistency of the estimated ambiguities is assured between the overlapping data arcs. This processing strategy turns out to be recommendable also for the AIUB product.

The DLR clock estimation algorithm has been designed as prototype software for a real-time clock estimation process. Still, some differences to a true real-time system exist, however, and shall be addressed here. First, differences in the orbit/clock-products may result from the geometry of the corresponding tracking networks. The JPL real-time tracking network with over 100 globally distributed stations will certainly provide the best coverage and observing geometry (Bar-Sever 2008). The station network used for the DLR product shown in Fig. 2 consists of 25 IGS stations, which have been chosen to provide global coverage. It has not been considered, however, whether these sites also provide real-time data streams. The AIUB product exclusively uses high-rate IGS stations. The size, global coverage and observing geometry of the network is comparable to the DLR network (Bock et al. 2008). The ESA network consists of 25 stations (not counting the backup-stations), which are capable of real-time data transmission (Zandbergen et al. 2006). Again, the coverage and observing geometry do not vary significantly from the DLR network. It must therefore be concluded, that the differences in the performance are not caused by differences in the observing geometry of the selected networks. However, a significant amount of data might be lost or arrive too late for processing due to network problems between the station and the real-time processing facility. These data losses can cause a degradation of the clock estimation accuracy, since the estimation of ambiguities is unnecessarily re-initialized. The accumulated daily Rinex files processed by DLR and the 15-min high-rate Rinex files processed by AIUB are in contrary generally not affected by frequent data gaps. Last, it should be mentioned that the ESA and JPL clock-estimation algorithms are implemented in operational environments and expected to deliver products with a reliable performance under all circumstances. Consequently, robustness has a higher priority than achieving the highest possible accuracy, as long as operational accuracy requirements are met.

The implemented offline filter for the DLR products is evidently suitable to produce high precision clock solutions. A real-time system for clock estimation (RETICLE) using the core algorithms of the offline filter is currently implemented. The algorithm produces clock solutions for the complete GPS constellation and processes data from NTRIP-streams of a global network, which are accessible through a participation in the real-time working group of IGS.

Acknowledgments The following contributions are gratefully acknowledged: Near real-time and real-time clocks and orbits for the analyses have been contributed by AIUB, ESOC (via Eumetsat) and JPL (via Infoterra). The final orbits and clocks have been obtained from CODE and the ultra-rapid predicted orbits and clocks from IGS. The GPS data from the GRAS receiver on MetOp-A has been made available by ESA/Eumetsat.

References

Bar-Sever Y (2008) The NASA Global Differential GPS System—System Description—Network. Accessible online: http://www.gdgps.net/system-desc/network.html. Accessed June 2008

Bar-Sever Y, Bell B, Dorsey A, Srinivasan J (2003) Space applications of the NASA global differential GPS system. Institute of Navigation. Portland, Oregon

Bock H, Dach R, Yoon Y, Montenbruck O (2008) GPS clock correction estimation for near real-time orbit determination applications. Aerosp Sci Technol (submitted)

Collins P, Langley R, LaMance J (1996) Limiting factors in tropospheric propagation delay error modelling for GPS airborne navigation. Proceedings of the Institute of Navigation 52nd annual meeting, Cambridge, Massachusetts, 19–21 June 1996, pp 519–528

Dach R, Hugentobler U, Fridez P, Meindl M (2007) Bernese GPS Software 5.0. Astronomical Institute, University of Bern

Hutsell S (1996) Relating the Hadamard variance to MCS Kalman filter clock estimation. 27th annual precise time and time interval (PTTI) applications and planning meeting, pp 291–301

IGS (2008) Weekly Sinex files, ftp://cddis.gsfc.nasa.gov/pub/gps/products. Accessed June 2008

McCarthy DD, Petit G (2004) IERS technical note No. 32 (2003). Verlag des Bundesamts für Kartographie und Geodäsie, Frankfurt am Main

Montenbruck O, van Helleputte T, Kroes R, Gill E (2005) Reduced dynamic orbit determination using GPS code and carrier measurements. Aerosp Sci Technol 9(3):261–271. doi:10.1016/j.ast.2005.01.003

Montenbruck O, Andres Y, Bock H, van Helleputte T, van den Ijssel J, Loiselet M, Marquardt C, Silvestrin P, Visser P, Yoon Y (2008) Tracking and orbit determination performance of the GRAS instrument on MetOp-A. GPS Solutions

Pérez J, Agrotis L, Fernández J, Garcia C, Dow J (2006) ESA/ESOC real time data processing. IGS Workshop 2006, Darmstadt, Germany

Schaer S, Steigenberger S (2006) Determination and use of GPS differential code bias values. IGS Workshop, Darmstadt, Germany

Senior K, Ray J, Beard R (2008) Characterization of periodic variations in the GPS satellite clocks. GPS Solut 12:211–255. doi:10.1007/s10291-008-0089-9

Schmid R, Steigenberger P, Gendt G, Ge M, Rothacher M (2007) Generation of a consistent absolute phase center correction model for GPS receiver and satellite antennas. J Geod 81(12):781–798. doi:10.1007/s00190-007-0148-y

Warren DLM, Raquet JF (2003) Broadcast vs. precise GPS ephemerides: a historical perspective. GPS Solut 7(3). doi:10.1007/s10291-003-0065-3

Wu JT, Wu SC, Hajj GA, Bertiger WI, Lichten SM (1993) Effects of antenna orientation on GPS carrier phase. Manuscr Geod 18:91–98

Zandbergen R, Ballereau A, Rojo E, Andres Y, Romero I, Garcia C, Dow J (2006) GRAS GSN near-real time data processing. IGS Workshop, Darmstadt, Germany

Author Biographies

André Hauschild is a PhD candidate at German Space Operations Center (GSOC) since April 2007. His current activities focus on real-time estimation of GPS satellite clocks. He received his diploma in mechanical engineering from Technical University at Braunschweig, Germany, in March 2007.

Dr. Oliver Montenbruck is head of the GNSS Technol-ogy and Navigation Group at DLR's German Space Operations Center, where he started to work as a flight dynamics analyst in 1987. His current research activi-ties comprise spaceborne GNSS receiver technology, autonomous navigation systems, spacecraft forma-tion flying and precise orbit determination.